IEEE Access
Multidisciplinary | Rapid Review | Open Access Journal

Received August 10, 2020, accepted August 23, 2020, date of publication August 26, 2020, date of current version September 18, 2020.

Digital Object Identifier 10.1109/ACCESS.2020.3019690

Online Identification of Intrinsic Load Current Dependent Position Estimation Error for Sensorless PMSM Drives

HECHAO WANG, (Member, IEEE), KAIYUAN LU, (Member, IEEE), DONG WANG, (Member, IEEE), AND FREDE BLAABJERG, (Fellow, IEEE)
Department of Energy Technology, Aalborg University, 9220 Aalborg, Denmark

Corresponding author: Kaiyuan Lu (klu@et.aau.dk)

This work was supported by the Innovation Fund Denmark through the Advanced Power Electronic Technology and Tools (APETT) Project.

ABSTRACT Low-speed sensorless control of Permanent Magnet Synchronous Machine (PMSM) faces an intrinsic problem of increased position estimation error with increased load. This phenomenon is due to changed magnetic saliency caused by the load current on the machine side. Therefore, such position estimation error, which deteriorates the drive performance, cannot be corrected by the sensorless algorithm itself; it has to be detected/compensated by other methods. In this article, an on-line identification method is proposed to detect reliably this load current dependent position estimation error. The unique features of the proposed method are its easy implementation and plug-and-play capability, without the needs of machine detailed flux map or extra devices such as a rotor locker; the detection process is very fast, so even with the q-axis current present, it will not cause noticeable rotor position change. Various experimental results are presented to validate the effectiveness of the proposed method.

INDEX TERMS PMSM, sensorless, position estimation error, cross-saturation effects, parameter independent, searching strategy.

I. INTRODUCTION

PMSM has been widely used in modern adjustable speed drives due to its well-known advantages of high efficiency, compact size and high torque density [1]. Field Oriented Control (FOC) is often adopted for effective control of the PMSM, where the rotor position information is required, which is referred to as the rotor magnetic field axis. Instead of using an encoder, various position observers have been extensively studied in the last few decades to achieve sensorless operation of the drive for reducing the cost and increasing the reliability.

Position observers are normally divided into two categories for operations at medium-high speed range and at zero-low speed range respectively [2]. For medium-high speed range operation, position observers often utilize the fundamental model of the PMSM. The main idea is to detect the rotor position information contained in the back-EMF and the permanent magnet flux linkage [3]–[8]. Full-order [4] or reduced-order [5] state observers may be used. This kind of observer is not suitable for zero-low speed application due to the low amplitude of the back-EMF when the speed is low. At zero-low speed range, the rotor magnetic saliency is utilized for the position estimation by injecting e.g. revolving [9]–[11] or pulsating carrier signals [12]–[14] in either stationary or rotary reference frames. However, independent of the sensorless algorithm chosen, there is an intrinsic error in the detected magnetic saliency between no load and loaded conditions [15]. The magnetic field produced by the load current may affect the saturation of the machine magnetic path, which is also known as cross-saturation effects [15], and consequently, the orientation of the machine magnetic saliency deviates from its no-load axis [16]. This load current dependent error is hard to be corrected by the position estimation algorithms themselves [28]. In order to achieve satisfactory sensorless control performance, identification and compensation of the load current dependent position estimation error are needed [28].

Existing studies in identifying the profile of the load current dependent position estimation error can be categorized into two types: off-line and on-line identifications. One solution of the off-line methods is to calculate the position estimation error using the profiles of the machine

The associate editor coordinating the review of this manuscript and approving it for publication was Kan Liu.

self- and mutual-inductances or machine d- and q-axes flux linkages by considering the self- and cross-saturation effects [18], [19]. Such inductance or flux profiles can be obtained experimentally with the assistance of an additional rotor-locking device [20]. Alternatively, this can be done indirectly by using finite element analysis tools [17], which require detailed knowledge of the machine that is often not available for many industrial applications and will suffer from manufacturing tolerances as well. The other possible solution is to measure the load current dependent position estimation error directly. This can be done by locking the rotor to a known position and detect the position estimation error under different load conditions using the selected injection-based position observers [21]. The idea behind this approach is straightforward. The position estimation error is the deviated estimated position caused by the load current when compared to the estimated position at zero load current condition. Since the rotor is locked, the rotor position cannot change when the load current is applied. Then, by subtracting the estimated position at no-load from the estimated position at a loaded condition, this load dependent position error can be identified. The main inconvenience of this approach is that with the load current present, the machine produces torque and it is necessary to lock the rotor using a rotor locking device in order to accomplish the test in such a way [20], [21]. An alternative off-line solution is to use the position estimated from the fundamental excitation-based position observer as a reference, since the influence of the cross-saturation effects is assumed to be limited in such position observers [22], [23]. However, to do so, the drive system needs to be operated at the medium-high speed range, which does not favor the signal injection methods due to e.g. the increased influences of the back-EMF voltage and increased fundamental frequency; manipulation of the load for identifying the position error at different load levels is also required, which complicates the test procedure.

Since the above-mentioned off-line methods require either detailed machine knowledge or an extra shaft locking device / load manipulation possibility, it is inconvenient or even impossible to be performed on-site for many industrial applications. Instead, on-line identification methods, without involving extra devices and influencing the machine operation conditions, are much preferred [24], [25]. Unfortunately, on-line identification methods have not been well researched so far (very few relevant references). One on-line solution proposed was to use a neural network algorithm applied in the steady state operation of the machine [24]. Its implementation complexity and calculation burden on the controller will be high. In practice, it is preferred to run this load current dependent position error detection in the initialization phase of the drive. Since typically, the position error is in a linear relationship to the load current. This can be easily stored as a look-up table for use in normal operations of the drive. It is worth to emphasize that the on-line identification algorithm in the initialization phase should not cause noticeable change of the rotor position, in order to avoid undesired movements of the load. To serve this purpose, attempt has been made in [25]. However, the proposed method in [25] requires detailed information of machine parameters in order to estimate the gain value between the q-axis current and the position estimation error; it uses parabolic curve fitting with the assumptions of small position estimation error, constant d- and q-axes inductances, neglected resistive voltage drop, etc. Since one of the attractive advantages of many injection-based position estimation algorithms is the machine parameter independency, a machine parameter independent position error identification method is much preferred. In [26], attempt has been made to find this position estimation error at start-up. But rotating voltage vector injected for 360 degrees are used, which is not convenient. To summarize, it is of great interest to develop an on-line identification method that is machine parameter independent, simple to implement, fast in response, and will not cause noticeable rotor rotation even with the load current (q-axis current) present. It should not require locking the rotor or manipulation of the load system in order to accomplish the position error identification. To the authors' knowledge, there are little efforts done so far towards such a plug-and-play solution.

In this article, a new active searching strategy is introduced to achieve a fast and reliable load-dependent position estimation error detection in the system initialization phase before machine start-up; the influence to the system initial condition is then minimized. The proposed approach is a plug-and-play solution without requiring detailed machine parameter information or a shaft locking device. The proposed method is verified experimentally, and the improved sensorless drive performance with this error compensated is illustrated.

This article is organized in the following manner. In section II, a typical high-frequency signal injection based sensorless drive system is briefly introduced. The influence of position estimation error caused by the load current is clearly demonstrated. In section III, the machine high-frequency model used for position estimation at zero-low speed range is presented and the influence of the load current to the machine high-frequency model and consequently the position estimation error is analyzed. In section IV, the proposed on-line identification procedure, including the adopted sensorless algorithm and proposed searching strategy, is explained in detail. An active searching strategy is investigated to fasten the identification procedure without causing any noticeable change of the rotor position. In section V, experimental verifications of the proposed on-line identification method are given. The performance of the sensorless drive with on-line identification and compensation of the load current dependent position error is provided to prove the feasibility and effectiveness of the entire control solution.

II. SENSORLESS CONTROL SYSTEM AND POSITION ESTIMATION ERROR PHENOMENON

A typical PMSM sensorless drive system based on FOC with $i_d = 0$ is shown in Fig. 1. The rotor position information, which is essential for transformations needed in the FOC

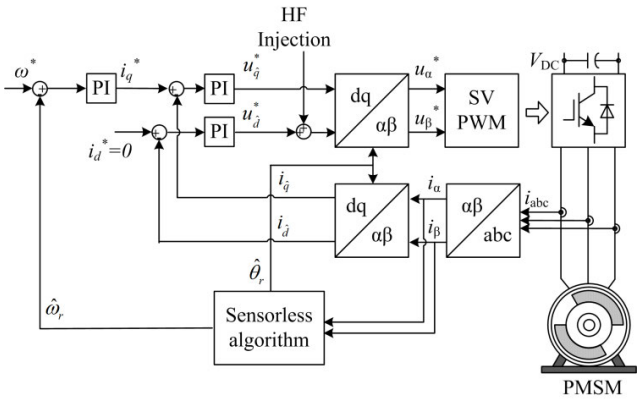

FIGURE 1. Sensorless FOC system for PMSM.

system, could be estimated by using high frequency signal injection methods. To minimize the influences of the uncertainties in motor terminal voltages and motor parameters on position estimation accuracy, the position estimation algorithm [13], which utilizes the motor phase currents only, is adopted in this article.

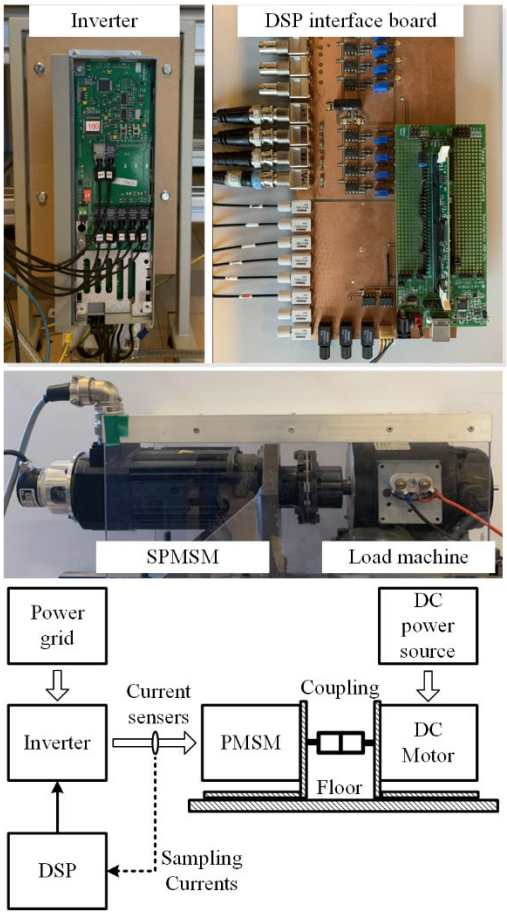

FIGURE 2. Experimental setup for testing the identification method.

The test setup is shown in Fig. 2. The parameters of the PMSM are listed in Table 1. A DC motor is connected to the PMSM to serve as the load machine. A Danfoss FC302

TABLE 1. Parameters of the used PMSM.

Parameters of PMSM	
Rated power [W]	400
Max. phase voltage [V]	380
Rated current (RMS) [A]	2.9
Rated speed [rpm]	2850
Rated frequency [Hz]	95
Stator resistance [Ω]	2.3
d-axis inductance [mH]	10
q-axis inductance [mH]	13
PM flux linkage [Wb]	0.12
Pole pairs	2
System inertia [kg·m^2]	1e-3

voltage source inverter is used to drive the PMSM, where the controller is implemented on a DSP-TMS320F28335 with a switching frequency of 5 kHz (same as the sampling frequency). An incremental encoder with 2048 lines per revolution is mounted on the non-drive-end of the PMSM to obtain actual rotor position and speed as reference signals for comparison with estimated position and speed. The injection voltage magnitude is chosen to be 50 V, compromising the signal-to-noise ratio and resultant injected current ripple [31].

Fig. 3 shows the performance of the PMSM drive using the estimated position as feedback under an operation condition

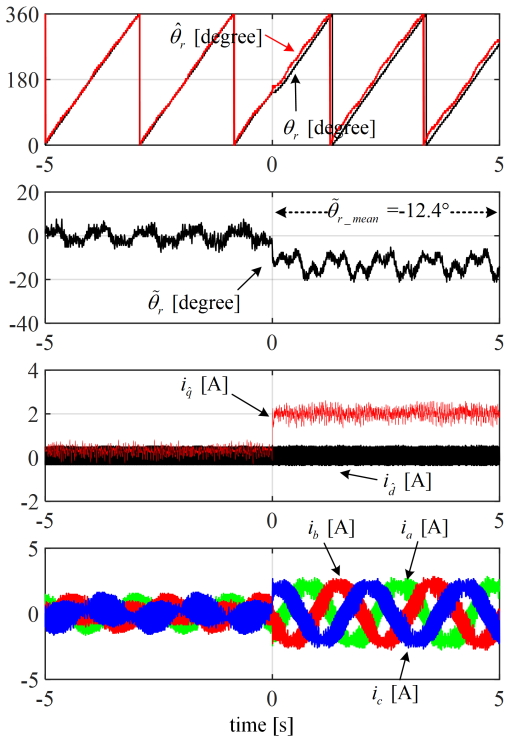

FIGURE 3. Experimental results of the position sensorless drive under 50% load torque step at 15 rpm without position error compensation. From top to bottom: mechanical and estimated rotor position, position error, machine currents in the estimated dq-frame, and 3-phase currents.

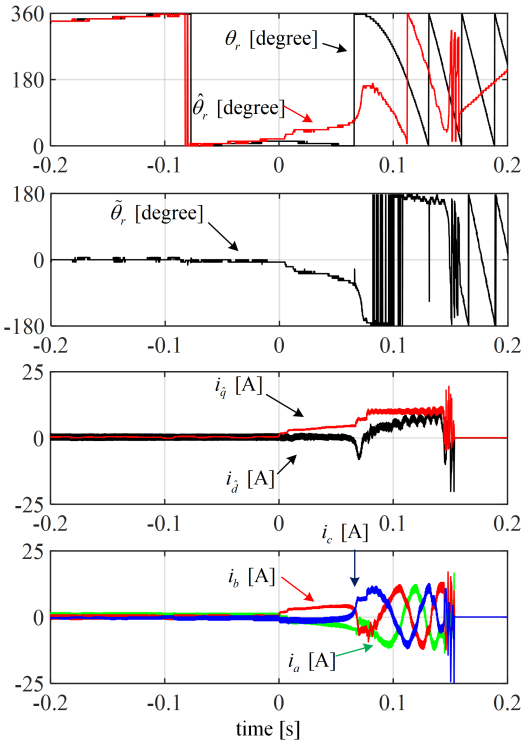

FIGURE 4. Experimental results of the position sensorless drive under 100% load torque step at 15 rpm without position error compensation. From top to bottom: mechanical and estimated rotor position, position error, machine currents in the estimated dq-frame, and 3-phase currents.

of 50% load torque step at 15 rpm. The drive can handle the half-load torque step change, as shown in Fig. 3. However, a large position estimation error of -12.4° in average can be observed, as the q-axis current increases to 2 A at 50% load torque. This error is due to the cross-saturation effects caused by the load current and will be further explained in section III.

The existence of this load current dependent position estimation error will degrade the drive performance. A large position estimation error will bring an unnecessary d-axis current component in the steady state operation. The situation will be worse when the load increases which results in increased position estimation error. For example, with a full load torque step as shown in Fig. 4, the controller is even not able to run the machine stably due to a too large position estimation error. Hence, this load dependent position estimation error must be carefully investigated and compensated.

III. LOAD DEPENDENT PMSM SMALL SIGNAL MODEL AND SENSORLESS SCHEME

The load current will distort the magnetic field and consequently the saturation condition of the machine, both self- and cross-saturation effects will appear [15]. Typical machine voltage equations in the dq-reference frame including the self- and cross-saturation effects can be expressed as:

$$\begin{bmatrix} u_d \\ u_q \end{bmatrix} = R\begin{bmatrix} i_d \\ i_q \end{bmatrix} + \frac{d}{dt}\begin{bmatrix} \lambda_d \\ \lambda_q \end{bmatrix} + \omega_r \begin{bmatrix} 0 & -1 \\ 1 & 0 \end{bmatrix}\begin{bmatrix} \lambda_d \\ \lambda_q \end{bmatrix}$$
$$\begin{bmatrix} \lambda_d \\ \lambda_q \end{bmatrix} = \begin{bmatrix} L_d & L_{dq} \\ L_{qd} & L_q \end{bmatrix}\begin{bmatrix} i_d \\ i_q \end{bmatrix} + \lambda_{mpm}\begin{bmatrix} 1 \\ 0 \end{bmatrix} \quad (1)$$

where u_d, u_q, i_d, i_q are the stator d- and q-axes voltages and currents respectively; L_d and L_q are the d- and q-axes inductances; L_{dq} and L_{qd} are the mutual inductances in dq-frame caused by the machine load currents; R is the stator resistance; ω_r is the rotor electrical speed; λ_d, λ_q are the d- and q-axes flux linkages, and λ_{mpm} is the amplitude of the rotor PM flux linkage. It should be noticed that L_{dq} and L_{dq} are i_d and i_q dependent, respectively (self-saturation); the mutual inductance L_{dq} and L_{qd} are i_d and i_q dependent (cross-saturation) and they are equal to each other [27].

When considering the machine small signal responses at much higher frequency than the machine fundamental frequency, it is safe to assume that the resistive voltage drop and the back-EMF voltage component does not change during two neighboring switching periods. Then according to [13], by applying (1) in the first and second switching periods respectively and then subtracting these two voltage equations, (1) is reduced to:

$$\begin{bmatrix} \Delta u_d \\ \Delta u_q \end{bmatrix} \approx \begin{bmatrix} L_d & L_{dq} \\ L_{dq} & L_q \end{bmatrix}\frac{d}{dt}\begin{bmatrix} \Delta i_d \\ \Delta i_q \end{bmatrix} \quad (2)$$

where Δ represents the difference between the two neighboring switching periods. In (2), the influences of uncertain voltage components such as the phase resistive voltage drop and back-EMF voltage component are removed due to the subtraction, giving simplified equations. Subtraction of the voltage equations in the two neighboring switching periods has been proven to be effective in suppressing these aforementioned voltage disturbances on position estimation accuracy [13].

A more convenient form to represent (2) is to get rid of the cross-coupling inductance L_{dq}. This can be achieved by transforming (2) to a special d′ q′ -reference frame that leads the real dq-frame by an angle of $\varepsilon = 0.5 \cdot \arctan[2L_{dq}/(L_d - Lq)]$, as indicated in Fig. 5. The angle ε between the d′ -axis and the mechanical d-axis is L_{dq} dependent, which is affected by the load current. Preforming reference frame transformation gives:

$$\begin{bmatrix} \Delta u_{d'} \\ \Delta u_{q'} \end{bmatrix} = \begin{bmatrix} L_{d'} & 0 \\ 0 & L_{q'} \end{bmatrix}\frac{d}{dt}\begin{bmatrix} \Delta i_{d'} \\ \Delta i_{q'} \end{bmatrix}$$
$$L_{d'} = (L_d + L_q)/2 - \left(\sqrt{(L_d - L_q)^2 + 4L_{dq}^2}\right)/2$$
$$L_{q'} = (L_d + L_q)/2 + \left(\sqrt{(L_d - L_q)^2 + 4L_{dq}^2}\right)/2 \quad (3)$$

and $u_{d'}$, $u_{q'}$, $i_{d'}$, $i_{q'}$ are the stator voltages and currents respectively in the d′ q′ -reference frame (Fig. 5). In (3), the d′ -, q′ -axes are mathematically decoupled. Therefore, the d′ -axis is considered as the machine apparent magnetic saliency. At no-load, $L_{dq} = 0$, and consequently $\varepsilon = 0$. The d′ -axis becomes aligned with the mechanical d-axis (Fig. 5), and the machine model (3) becomes the classical machine dq-model since $L_{d'}$ and $L_{q'}$ can be simplified to L_d and L_q respectively with $L_{dq} = 0$ in (3).

When considering sensorless operation, since only estimated position information could be obtained, the

estimated $\hat{d}\hat{q}$-reference frame, where the signal is injected to, needs to be introduced and is shown in Fig. 5.

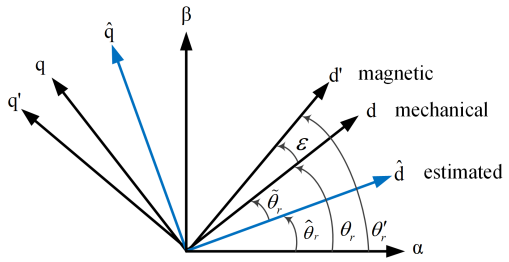

FIGURE 5. Relationship among different reference frames: d-axis is the mechanical (rotor magnetic) axis; d′ -axis is the machine magnetic axis and $\hat{d}$ -axis is the estimated rotor axis.

Then by transforming (3) to the estimated $\hat{d}\hat{q}$-frame, (4) can be obtained:

$$\begin{bmatrix} \Delta u_{\hat{d}} \\ \Delta u_{\hat{q}} \end{bmatrix} = \begin{bmatrix} L_0 + L_1 \cos 2(\tilde{\theta}_r + \varepsilon) & L_1 \sin 2(\tilde{\theta}_r + \varepsilon) \\ L_1 \sin 2(\tilde{\theta}_r + \varepsilon) & L_0 - L_1 \cos 2(\tilde{\theta}_r + \varepsilon) \end{bmatrix} \frac{d}{dt} \begin{bmatrix} \Delta i_{\hat{d}} \\ \Delta i_{\hat{q}} \end{bmatrix} \tag{4}$$

where $u_{\hat{d}}, u_{\hat{q}}, i_{\hat{d}}, i_{\hat{q}}$ are the stator voltages and currents respectively in the $\hat{d}\hat{q}$-reference frame; $L_0 = (L_{d'} + L_{q'})/2$, and $L_1 = (L_{d'} - L_{q'})/2$; $\tilde{\theta}_r$ is the position estimation error between the mechanical rotor position (θ_r) and the estimated rotor position ($\hat{\theta}_r$), i.e. $\tilde{\theta}_r = \theta_r - \hat{\theta}_r$ as indicated in Fig. 5. However, based on (4), it is clear that only $\tilde{\theta}_r + \varepsilon$ can be obtained by manipulating the equations. This means based on the estimated $\hat{d}$-axis and the obtained position estimation error, only the magnetic d′ -axis can be identified. This feature is independent on the injection scheme chosen. The desired position error between the estimated and machine mechanical d-axis $\tilde{\theta}_r$ cannot be obtained without the knowledge of ε.

A sensorless algorithm needs to be chosen first for the normal operation of the machine. Due to advantages of simple implementation, no requirement of any filters and the ability to suppress disturbing voltage components, in this article, two opposite voltage vectors aligned with the estimated $\hat{d}$-axis ($\pm\vec{V}_{\hat{d}}$, Fig. 6) are injected during two consequent switching periods, where the injection frequency is 2.5 kHz. Under this condition, it can be obtained from (4) (i.e. $\Delta u_{\hat{d}} = 2V_{\hat{d}}$ and $\Delta u_{\hat{q}} = 0$ in (4)) that [13]:

$$\frac{d\Delta i_{\hat{q}}}{dt} \approx \frac{\Delta(\Delta i_{\hat{q}})}{T_s} = \frac{-L_1 \Delta u_{\hat{d}}}{L_0^2 - L_1^2} \sin(2\tilde{\theta}_r + 2\varepsilon) \tag{5}$$

where T_s is the switching period. The differential $d\Delta i_{\hat{q}}/dt$ can be approximated by $\Delta(\Delta i_{\hat{q}})/T_s$. It can be seen that the position information $\sin(2\tilde{\theta}_r + 2\varepsilon)$ can be obtained by measuring the variation of the $\hat{q}$-axis current change rates during two neighboring switching periods. Thus, the position error between the estimated and real d-axes $\tilde{\theta}_r$ can be obtained only if ε is known. Sensorless operation of the drive is not the focus of this article, more detailed information of this sensorless method can be found in [13].

IV. LOAD DEPENDENT POSITION ESTIMATION ERROR IDENTIFICATION

A. LOAD DEPENDENT POSITION ESTIMATION ERROR DETECTION PROCEDURE

As pointed out in the above section, a load/saturation dependent position estimation error ε exists when utilizing the machine high frequency model to detect the rotor position. The error can be significant and should be identified and compensated to achieve satisfactory sensorless control performance. In this section, an on-line identification method to find ε, which is implemented in the initialization phase before machine start-up, is proposed. The obtained relationship between ε and the load current may then be conveniently used to correct the estimated position used for normal sensorless operation of the drive. In this article, to illustrate this identification method, i_d is kept to be zero since ε is mainly dependent on the i_q.

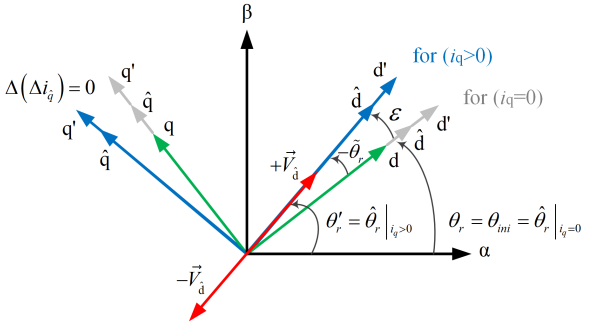

FIGURE 6. Comparison of different injection methods for rotor position estimation.

When the estimated $\hat{d}$-axis is aligned with the magnetic d'-axis, the injected voltage will result in zero current variation on the estimated q'-axis (i.e.$\Delta(\Delta i_{\hat{q}}) = 0$), since this results in $\varepsilon = -\tilde{\theta}_r = \hat{\theta}_r - \theta_r$ according to (5), and the corresponding locations of the axes are illustrated in Fig. 6 (for the case of $i_q > 0$). Noting that the position estimation error $\tilde{\theta}_r$ is defined to be positive when the estimated $\hat{d}$-axis is lagging the real d-axis (Fig. 5), so here $\tilde{\theta}_r$ is indicated as $-\tilde{\theta}_r$ for the leading $\hat{d}$-axis position with respect to the real d-axis shown in Fig. 6. It is worth to point out that there is only one equation (5) available but there are two unknown variables (ε and $\tilde{\theta}_r$). Other measures must be used in order to determine ε.

At no-load, the load dependent position errorε is zero. The initial rotor position (θ_{r0}) may be unknown, but it can be estimated by using the adopted sensorless algorithm, denoted as $\hat{\theta}_r\big|_{i_q=0}$. If it is assumed that the estimated initial position at no-load is $\hat{\theta}_r\big|_{i_q=0} = \theta_{r0}$, then when the load current increases ($i_q > 0$) and if the rotor position cannot change, there will occur a position estimation error $\tilde{\theta}_r$ with respect to the position estimated at no-load, which will satisfy $\varepsilon = -\tilde{\theta}_r = \hat{\theta}_r\big|_{i_q>0} - \hat{\theta}_r\big|_{i_q=0}$ if the estimated $\hat{d}$-axis keeps tracking the magnetic d′ -axis by searching for the position that makes $\Delta(\Delta i_{\hat{q}}) = 0$ (Fig. 6). The load dependent position error ε can then be obtained for different load conditions in such a way.

In practice, due to measurement noise, the measured current variation could not be really zero. Therefore, searching for the minimal $\left|\Delta(\Delta i_{\hat{q}})\right|$ is used. This is preferred instead of calculating ε directly by using (5) from measured $\Delta(\Delta i_{\hat{q}})$ and $\tilde{\theta}_r$, since the searching method does not need to know the gain factor (determined by machine parameters) involved in the right side of (5). The searching method will converge to an injection position $\hat{\theta}_r$ that can make $\Delta(\Delta i_{\hat{q}})$ (and consequently $\sin(2\tilde{\theta}_r+2\varepsilon)$) to be ideally zero. Under this condition, no matter how large the gain factor (including injected voltage magnitude) is, $\varepsilon = -\tilde{\theta}_r$. In this approach, the values of the machine parameters and injected voltage magnitudes are not needed in achieving the converged position by the searching method.

In the above analysis, it is assumed that $\hat{\theta}_r\,|_{i_q=0} = \theta_{r0}$, i.e. the initial position estimation is accurate enough. To validate this, the performance of the initial position detection by using the $\hat{d}$-axis opposite voltage injection method is investigated and the results are shown in Fig. 7. It can be seen that the position detection errors at different rotor initial positions at no-load are all within ± 3 electrical degrees, which are not significant for sensorless control.

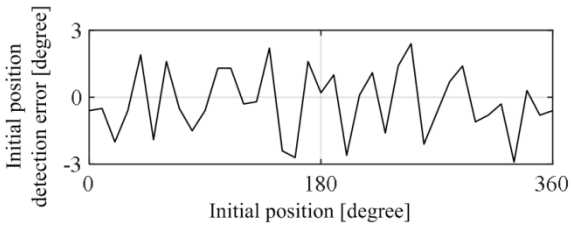

FIGURE 7. Initial position detection error.

It may be further mentioned that since the initial position detection and load dependent position error detection use the same algorithm, the possible detection error of the initial position (caused by the algorithm itself) will be there when performing the load dependent position error detection. The desired load dependent position error to be obtained is the incremental position change between a loaded condition and the no-load condition (initial position). Therefore, the position error vs. load current profile is not affected by the inherent position error contained in the algorithm itself which affects the initial position detection. It is clear from the obtained $\varepsilon - i_q$ curve shown in the following section that when the q-axis current is zero, $\varepsilon = 0$ (no error).

To summarize, the implementation of the above described procedure for the load dependent position error ε detection is illustrated in Fig. 8. The first step is an initial d-axis position detection to obtain θ_{r0} at zero q-axis current; the second step is to adjust i_q to an expected value (a loaded condition); at last opposite voltage vectors on the estimated $\hat{d}$-axis are injected and corresponding $\Delta(\Delta i_{\hat{q}})$ is obtained. As may be observed from Fig. 8, it takes two switching periods only for completing $\pm\vec{V}_{\hat{d}}$ injection to obtain the desired $\Delta(\Delta i_{\hat{q}})$ value and one more switching period to maintain the desired q-axis

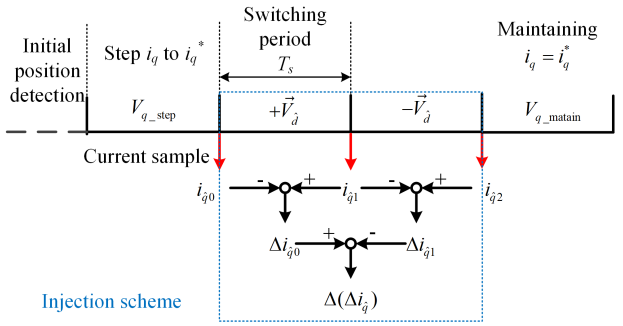

FIGURE 8. Procedure of proposed detection method for rotor position estimation.

current. During the whole detection period, a certain q-axis current needs to be maintained to create the loaded saturation condition whereas the corresponding load dependent position error ε is determined by the searching method to find minimal $\left|\Delta(\Delta i_{\hat{q}})\right|$ that is to be discussed below.

B. SEARCHING STRATEGY

An important requirement mentioned in the above analysis is that the rotor position should be kept unchanged for both no-load and loaded conditions, without locking the rotor. In detecting ε when certain q-axis current (i_q) is maintained, the machine is generating torque and will start to rotate if the generated torque is higher than the system static frictional torque. Since the machine mechanical time constant is often much larger than its electrical time constant, it is possible to maintain the rotor position if the detection algorithm with this bias q-axis current i_q present could be implemented in a very short duration (e.g. few switching periods).

To fasten the identification procedure, secant method is employed in this article. It should be noted that ε is zero when i_q is zero, ε is positive when i_q is positive, and vice versa. Then, since typically $|\varepsilon| < 45°$ [28], for the positive i_q bias current, it is convenient and safe to choose two initial values of the secant method as the initial position of 0° in this example study and another position at 45° away – an assumed large position estimation error possibly affected by the q-axis current. Similarly, the two initial values are chosen to be 0° and -45° for negative q-axis bias current.

The first two iterations of the secant method when $i_q = 4$ A are shown in Fig. 9. The two initial injection positions ($\hat{\theta}_{r1}$ and $\hat{\theta}_{r2}$) are chosen to be $\hat{\theta}_{r0} + 0°$ and $\hat{\theta}_{r0} + 45°$ respectively, where $\hat{\theta}_{r0}$ is the detected initial position as described in the above subsection. Two $\Delta(\Delta i_{\hat{q}})$ values could be obtained by injecting voltage pulses on the axes located at $\hat{\theta}_{r1}$ and $\hat{\theta}_{r2}$ respectively, which are points A and B as shown in the top plot of Fig. 10. The first secant line S_1 that links points A and B has a zero-crossing point at $\hat{\theta}_{r3} = \hat{\theta}_{r0} + 23.0°$, which is denoted by point C (hollow dot point) as shown in the zoomed bottom figure of Fig. 10. Then the voltage vector is injected on $\hat{\theta}_{r3}$ axis and the actual value of $\Delta(\Delta i_{\hat{q}})$ can be obtained, which is denoted by point D (solid dot point). Thereafter,

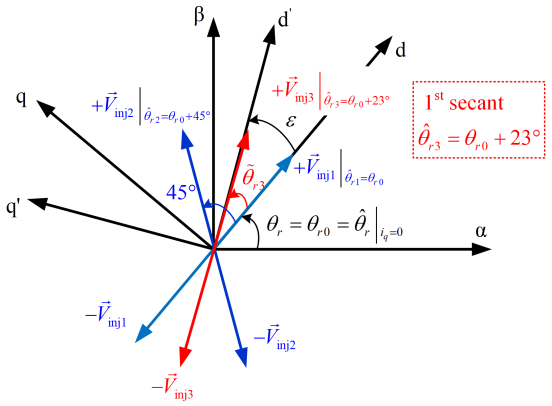

FIGURE 9. Demonstration of the voltage injections used during the 1st secant iteration of the proposed secant searching method.

the second secant line S_2 linking point D and point A (since $|\Delta(\Delta i_{\hat{q}})|_{\text{point A}} < |\Delta(\Delta i_{\hat{q}})|_{\text{point B}}$ in this case study) can then be formed to find the zero-crossing point E at $\hat{\theta}_{r4}$ as shown in Fig. 10. The iteration can be repeated to narrow down the searching range. It is found that the iteration converges at $\hat{\theta}_{r5} = \hat{\theta}_{r0} + 24.4°$, linearly interpolated from the third and fourth injection results of the iterations, since the variation of the detected position is less than 0.1° for continued iterations.

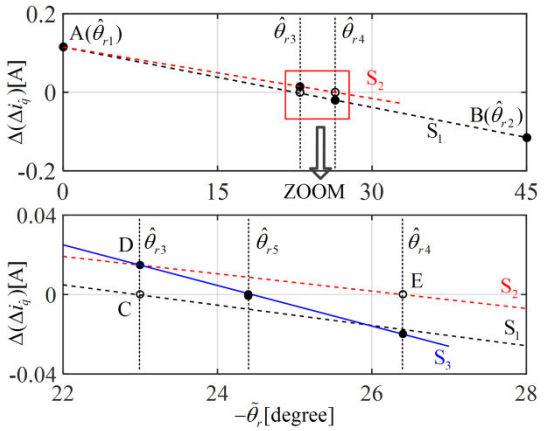

FIGURE 10. Procedure of the proposed secant searching method for finding the desired position error (hollow dot point: from interpolation; solid dot point: from $\Delta(\Delta i_{\hat{q}})$).

As mentioned before, three switching periods are needed for the injection at a selected rotor position ($\pm\vec{V}_{\hat{d}}$ injection followed by one more switching period for maintaining the q-axis current). Therefore, after obtaining $\hat{\theta}_{r5}$, only 15 switching periods (3 ms) are needed for completing the searching algorithm. It should be noted here that even after the first two injections giving points A and B (6 switching periods), the obtained position from iteration is $\hat{\theta}_{r3} = \hat{\theta}_{r0} + 23.0°$. There is only 1.4° difference compared to the converged value. This searching method is very fast to converge.

By using the searching strategy discussed above, the load/saturation dependent position estimation error at different i_q values ($\varepsilon - i_q$ relationship) can be obtained for different initial rotor positions through experiments and the results are shown in Fig. 11. It can be seen that they agree well with each other. An extra experiment is performed with the assistance of a shaft locker as shown in Fig. 12. It can be observed that the result obtained with a shaft locker is similar to the result from the proposed identification method without the need to lock the rotor. Moreover, the sensorless algorithm based on (5) is tested during normal rotational operation conditions and different loads are applied. The position errors between the estimated and actual rotor positions (obtained from an encoder), which are mainly caused by the load current cross-saturation effects, is obtained and shown in Fig. 12. It matches well with the proposed on-line method obtained at standstill conditions.

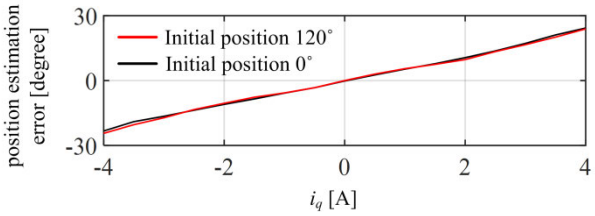

FIGURE 11. Measurement result of the q-axis current dependent position error obtained from the secant searching method at different initial positions.

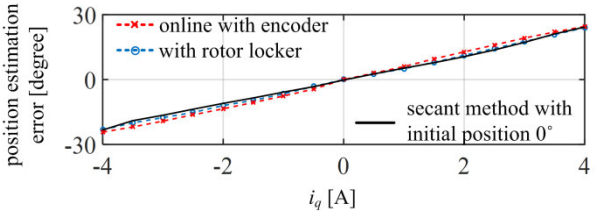

FIGURE 12. Comparison of the measured q-axis current dependent position errors from a locked rotor test, the rotating test using the encoder position as the reference, and from the proposed secant searching method.

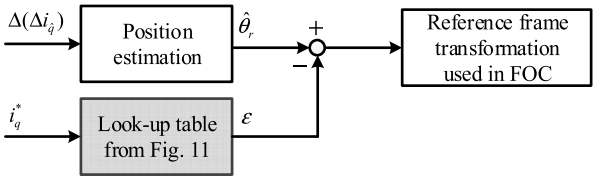

FIGURE 13. Block diagram of the position error compensation.

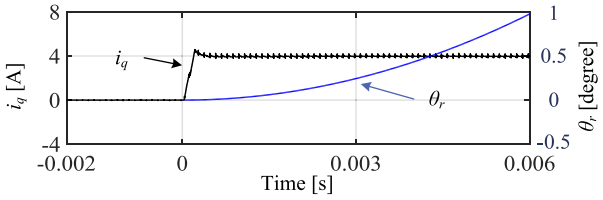

FIGURE 14. Rotor position change when q-axis current is applied.

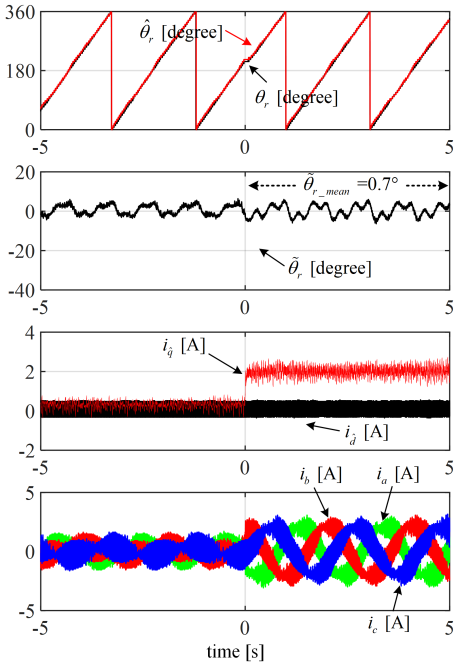

FIGURE 15. Experimental results of the sensorless drive with estimated position feedback under 50% load torque step at 15 rpm with position error compensation. From top to bottom: mechanical and estimated rotor position, position error, machine currents in the $\hat{d}\hat{q}$-frame, and 3-phase currents.

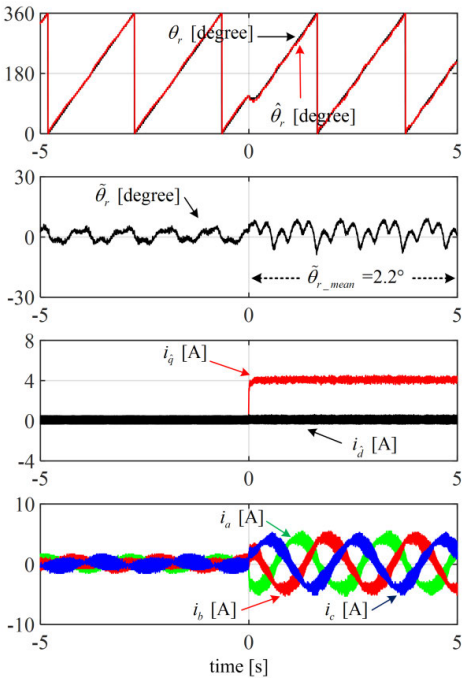

FIGURE 16. Experimental results of the sensorless drive with estimated position feedback under 100% load torque step at 15 rpm with position error compensation. From top to bottom: mechanical and estimated rotor position, position error, machine currents in the $\hat{d}\hat{q}$-frame, and 3-phase currents.

The obtained $\varepsilon - i_q$ relationship may be involved in the sensorless control as a simple look-up table and is used to compensate the estimated position as illustrated in Fig. 13.

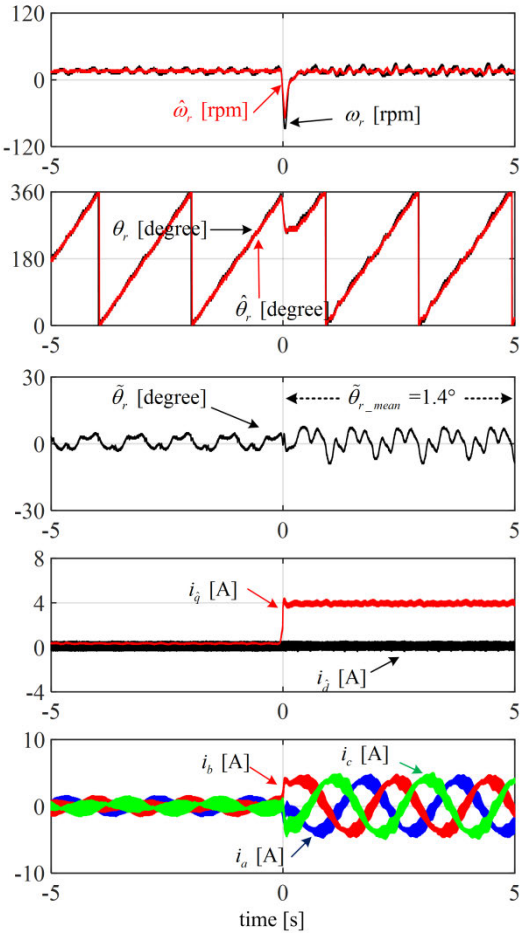

FIGURE 17. Experimental results of full sensorless drive under 100% load torque step at 15 rpm with position error compensation. From top to bottom: real and estimated speed, mechanical and estimated rotor position, position error, machine currents in the $\hat{d}\hat{q}$-frame, and 3-phase currents.

V. EXPERIMENT VERIFICATION

A. DETERMINATION OF IDENTIFICATION TIME DURATION

To verify the discussion regarding the maximum allowable identification time duration in section IV.B, an experiment is carried out with 4 A q-axis current. It can be seen from Fig. 14 that it takes about 6 ms for the rotor to rotate for one electrical degree. This means that if $\theta_{\max} = 1°$ and $i_q = 4$ A, the identification procedure is allowed to use about 30 switching periods to detect the load dependent position estimation error ε for the setup shown in Fig. 2.

B. VERIFICATION OF IDENTIFIED ε-i_q RELATIONSHIP

The $\varepsilon - i_q$ relationship (look-up table) obtained in section IV.B is used to correct the estimated position as shown in Fig. 13. Fig. 15 shows the performance of the PMSM drive using the corrected position estimation as feedback under an operation condition of 50% load torque step at 15 rpm. It can be observed that when the $\varepsilon - i_q$ compensation is involved, the position estimation error $\tilde{\theta}_r$ is only 0.7° in average, which shows the effectiveness of the compensation

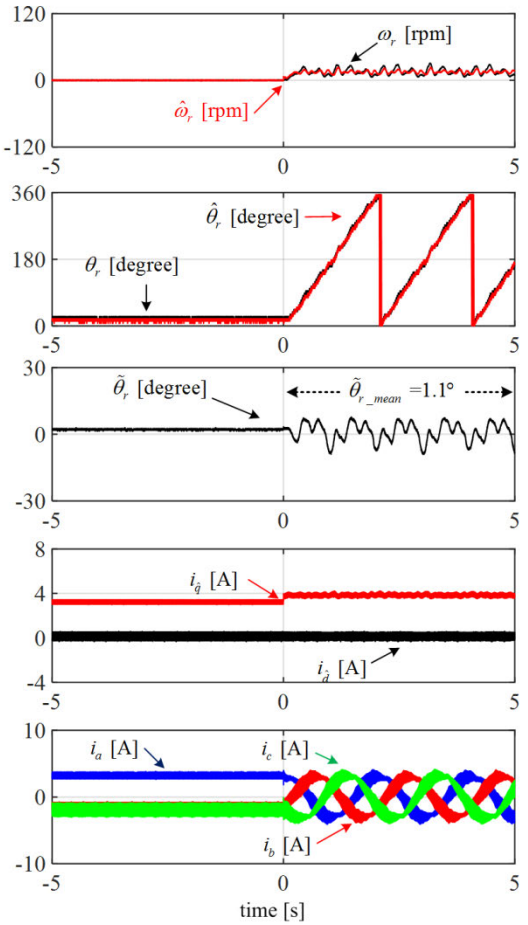

FIGURE 18. Experimental results of full sensorless drive with 0 rpm to 15 rpm speed step change at constant full load condition with position error compensation. From top to bottom: real and estimated speed, mechanical and estimated rotor position, position error, machine currents in the $\hat{d}\hat{q}$-frame, and 3-phase currents.

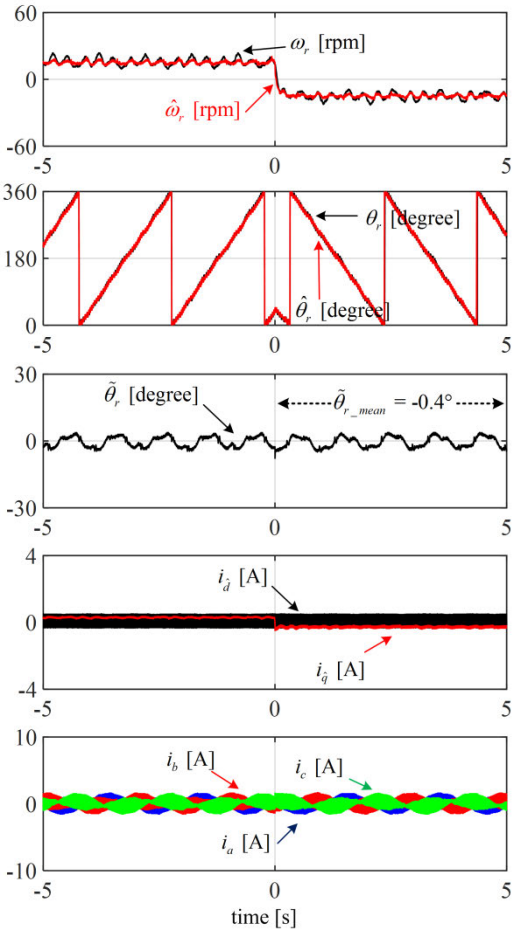

FIGURE 19. Experimental results of full sensorless drive with speed reversal from 15 rpm to -15 rpm with position error compensation. From top to bottom: real and estimated speed, mechanical and estimated rotor position, position error, machine currents in the $\hat{d}\hat{q}$-frame, and 3-phase currents.

and the correctness of the identified $\varepsilon - i_q$ relationship when compared with the previous experimental results under the same operation condition (-12.4° shown in Fig. 3).

Fig. 16 shows the performance of the PMSM drive using the corrected position estimation as feedback under a full load torque step at 15 rpm. Rather than losing the system stability without $\varepsilon - i_q$ compensation (as shown in Fig. 4), the sensorless drive can perform well with an average position estimation error of 2.2° only when $\varepsilon - i_q$ compensation is involved.

C. PERFORMANCE OF FULL SENSORLESS CONTROL WITH ε-i_q COMPENSATION

The performance of the PMSM drive with full sensorless control (both position and speed estimations are used as feedback signals in FOC) and $\varepsilon - i_q$ compensation at different operating conditions are shown in Fig. 17 to Fig. 19. Fig. 17 shows the experimental results under a full load torque step change at 15 rpm. The drive performs well with an average position estimation error of 1.4°.

Fig. 18 shows the experimental results when the reference speed of the drive steps from 0 rpm to 15 rpm at full load torque condition, where $\tilde{\theta}_r$ is only 1.1° in average. Fig. 19 shows the experimental results when the reference speed is reversed from 15 rpm to -15 rpm, where $\tilde{\theta}_r$ is only -0.4° in average.

VI. CONCLUSION

In this article, the influence of the load current dependent position estimation error of a sensorless drive is analyzed. A fast searching method for identifying such position error without the assistance of extra devices, setup modifications or machine inductance / flux map knowledge, is presented. The proposed plug-and-play load dependent position estimation error identification method is machine parameter independent and can be performed on-line at the system initialization phase before the machine start-up, without causing noticeable rotor position changes even with the rated q-axis current present. The relationship of the load/saturation dependent position estimation error versus q-axis current ($\varepsilon - i_q$) of a PMSM drive is obtained by using the proposed

identification method. It is shown by experiments that the position estimation error can be reduced greatly by compensating the estimated position with the obtained $\varepsilon - i_q$ relationship. Satisfactory results are obtained and the robustness of the sensorless drive is enhanced with the identified load current dependent position estimation error compensated. The drive system could handle tough conditions, such as full load step at low speed, full load starting and speed reversing.

REFERENCES

[1] S. Morimoto, K. Kawamoto, M. Sanada, and Y. Takeda, "Sensorless control strategy for salient-pole PMSM based on extended EMF in rotating reference frame," *IEEE Trans. Ind. Appl.*, vol. 38, no. 4, pp. 1054–1061, Jul. 2002.

[2] Y. Zhao, C. Wei, Z. Zhang, and W. Qiao, "A review on position/speed sensorless control for permanent-magnet synchronous machine-based wind energy conversion systems," *IEEE J. Emerg. Sel. Topics Power Electron.*, vol. 1, no. 4, pp. 203–216, Dec. 2013.

[3] I. Boldea, M. C. Paicu, and G.-D. Andreescu, "Active flux concept for motion-sensorless unified AC drives," *IEEE Trans. Power Electron.*, vol. 23, no. 5, pp. 2612–2618, Sep. 2008.

[4] J. Solsona, M. I. Valla, and C. Muravchik, "Nonlinear control of a permanent magnet synchronous motor with disturbance torque estimation," *IEEE Trans. Energy Convers.*, vol. 15, no. 2, pp. 163–168, Jun. 2000.

[5] J.-S. Kim and S.-K. Sul, "High performance PMSM drives without rotational position sensors using reduced order observer," in *Proc. 13th IEEE Ind. Appl. Conf., IAS Annu. Meeting*, Orlando, FL, USA, Oct. 1995, pp. 75–82.

[6] D. Liang, J. Li, R. Qu, and W. Kong, "Adaptive second-order sliding-mode observer for PMSM sensorless control considering VSI nonlinearity," *IEEE Trans. Power Electron.*, vol. 33, no. 10, pp. 8994–9004, Oct. 2018.

[7] X. Sun, J. Cao, G. Lei, Y. Guo, and J. Zhu, "Speed sensorless control for permanent magnet synchronous motors based on finite position set," *IEEE Trans. Ind. Electron.*, vol. 67, no. 7, pp. 6089–6100, Jul. 2020.

[8] X. Sun, C. Hu, G. Lei, Z. Yang, Y. Guo, and J. Zhu, "Speed sensorless control of SPMSM drives for EVs with a binary search algorithm-based phase-locked loop," *IEEE Trans. Veh. Technol.*, vol. 69, no. 5, pp. 4968–4978, May 2020.

[9] M. W. Degner and R. D. Lorenz, "Using multiple saliencies for the estimation of flux, position, and velocity in AC machines," *IEEE Trans. Ind. Appl.*, vol. 34, no. 5, pp. 1097–1104, Sep./Oct. 1998.

[10] M. J. Corley and R. D. Lorenz, "Rotor position and velocity estimation for a salient-pole permanent magnet synchronous machine at standstill and high speeds," *IEEE Trans. Ind. Appl.*, vol. 34, no. 4, pp. 784–789, Jul./Aug. 1998.

[11] M. Seilmeier and B. Piepenbreier, "Sensorless control of PMSM for the whole speed range using two-degree-of-freedom current control and HF test current injection for low-speed range," *IEEE Trans. Power Electron.*, vol. 30, no. 8, pp. 4394–4403, Aug. 2015.

[12] M. Schroedl, "Sensorless control of AC machines at low speed and standstill based on the 'INFORM' method," in *Proc. 31st Conf. Rec. IEEE Ind. Appl. Conf. Annu. Meeting (IAS)*, San Diego, CA, USA, Oct. 1996, pp. 270–277.

[13] H. Wang, K. Lu, D. Wang, and F. Blaabjerg, "Investigation of various position estimation accuracy issues in pulse-injection-based sensorless drives," in *Proc. Int. Power Electron. Conf. (IPEC-Niigata-ECCE Asia)*, Niigata, Japan, May 2018, pp. 1246–1252.

[14] M. Linke, R. Kennel, and J. Holtz, "Sensorless speed and position control of synchronous machines using alternating carrier injection," in *Proc. IEEE Int. Electric Mach. Drives Conf. (IEMDC)*, Madison, WI, USA, Jun. 2003, pp. 1211–1217.

[15] J. M. Liu and Z. Q. Zhu, "Novel sensorless control strategy with injection of high-frequency pulsating carrier signal into stationary reference frame," *IEEE Trans. Ind. Appl.*, vol. 50, no. 4, pp. 2574–2583, Jul. 2014.

[16] S. Øverbø, R. Nielsen, and R. Nielssen, "Saliency modeling in radial flux permanent magnet synchronous machines," in *Proc. NORPIE*, Trondheim, Norway, 2004, pp. 1–6.

[17] Z. Q. Zhu, Y. Li, D. Howe, and C. M. Bingham, "Compensation for rotor position estimation error due to cross-coupling magnetic saturation in signal injection based sensorless control of PM brushless AC motors," in *Proc. IEEE Int. Electric Mach. Drives Conf.*, Antalya, Turkey, May 2007, pp. 208–213.

[18] M. Hinkkanen, P. Pescetto, E. Molsa, S. E. Saarakkala, G. Pellegrino, and R. Bojoi, "Sensorless self-commissioning of synchronous reluctance motors at standstill," in *Proc. 22nd Int. Conf. Electr. Mach. (ICEM)*, Lausanne, Switzerland, Sep. 2016, pp. 1174–1180.

[19] A. Yousefi-Talouki, P. Pescetto, and G. Pellegrino, "Sensorless direct flux vector control of synchronous reluctance motors including standstill, MTPA, and flux weakening," *IEEE Trans. Ind. Appl.*, vol. 53, no. 4, pp. 3598–3608, Jul. 2017.

[20] S. Ebersberger and B. Piepenbreier, "Identification of differential inductances of permanent magnet synchronous machines using test current signal injection," in *Proc. Int. Symp. Power Electron. Power Electron., Electr. Drives, Autom. Motion*, Sorrento, Italy, Jun. 2012, pp. 1342–1347.

[21] N. Teske, G. M. Asher, M. Sumner, and K. J. Bradley, "Suppression of saturation saliency effects for the sensorless position control of induction motor drives under loaded conditions," *IEEE Trans. Ind. Electron.*, vol. 47, no. 5, pp. 1142–1150, Oct. 2000.

[22] P. Landsmann, D. Paulus, and R. Kennel, "Online identification of load angle compensation for anisotropy based sensorless control," in *Proc. Symp. Sensorless Control Electr. Drives*, Birmingham, U.K., Sep. 2011, pp. 80–84.

[23] K. Wiedmann and A. Mertens, "Self-sensing control of PM synchronous machines including online system identification based on a novel MRAS approach," in *Proc. 3rd IEEE Int. Symp. Sensorless Control Electr. Drives (SLED)*, Milwaukee, WI, USA, Sep. 2012, pp. 21–22.

[24] D. Diaz Reigosa, P. Garcia, D. Raca, F. Briz, and R. D. Lorenz, "Measurement and adaptive decoupling of cross-saturation effects and secondary saliencies in sensorless controlled IPM synchronous machines," *IEEE Trans. Ind. Appl.*, vol. 44, no. 6, pp. 1758–1767, Nov. 2008.

[25] P. Landsmann and R. Kennel, "Q-axis pulse based identification of the anisotropy displacement over load for surface mounted PMSM," in *Proc. IEEE Int. Symp. Sensorless Control Electr. Drives Predictive Control Electr. Drives Power Electron. (SLED/PRECEDE)*, Munich, Germany, Oct. 2013, pp. 1–6.

[26] H. Wang, K. Lu, D. Wang, and F. Blaabjerg, "Identification of load current influences on position estimation errors for sensorless SPMSM drives," in *Proc. IEEE Appl. Power Electron. Conf. Exposit. (APEC)*, San Antonio, TX, USA, Mar. 2018, pp. 533–539.

[27] D. Mingardi, M. Morandin, S. Bolognani, and N. Bianchi, "On the proprieties of the differential cross-saturation inductance in synchronous machines," *IEEE Trans. Ind. Appl.*, vol. 53, no. 2, pp. 991–1000, Mar. 2017.

[28] P. Guglielmi, M. Pastrorelli, and A. Vagati, "Cross saturation effects in IPM motors and related impact on zero-speed sensorless control," in *Proc. 14th IAS Annu. Meeting. Conf. Rec. Ind. Appl. Conf.*, Hong Kong, 2005, pp. 2546–2552.

[29] C. Li, G. Wang, G. Zhang, and D. Xu, "Eliminating position estimation error caused by cross-coupling effect in saliency-based sensorless control of SynRMs," in *Proc. 21st Int. Conf. Electr. Mach. Syst. (ICEMS)*, Jeju, South Korea, Oct. 2018, pp. 1600–1605.

[30] Z. Zhang and L. Xu, "Dead-time compensation of inverters considering snubber and parasitic capacitance," *IEEE Trans. Power Electron.*, vol. 29, no. 6, pp. 3179–3187, Jun. 2014.

[31] R. Mizutani, T. Takeshita, and N. Matsui, "Current model-based sensorless drives of salient-pole PMSM at low speed and standstill," *IEEE Trans. Ind. Appl.*, vol. 34, no. 4, pp. 841–846, Aug. 1998.

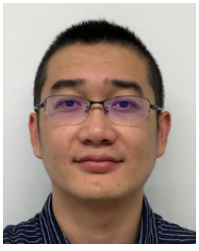

HECHAO WANG (Member, IEEE) received the B.S. and M.S. degrees from Tianjin University, Tianjin, China, in 2009 and 2014, respectively, and the Ph.D. degree from Aalborg University, Denmark, in 2019, all in electrical engineering.

From 2009 to 2010, he was with Shanghai Electric Machinery Company, Ltd., Shanghai, China, as a Motor Engineer. His research interest includes the control of synchronous reluctance and permanent magnet machines.

KAIYUAN LU (Member, IEEE) received the B.S. and M.S. degrees from Zhejiang University, Zhejiang, China, in 1997 and 2000, respectively, and the Ph.D. degree from Aalborg University, Denmark, in 2005, all in electrical engineering.

In 2005, he became an Assistance Professor with the Department of Energy Technology, Aalborg University, where he has been an Associate Professor, since 2008. His research interests include the design of permanent magnet machines, finite element method analysis, and control of permanent magnet machines.

DONG WANG (Member, IEEE) received the B.S. degree from Zhejiang University, Zhejiang, China, in 2004, and the M.S. and Ph.D. degrees from Aalborg University, Denmark, in 2006 and 2016, respectively, all in electrical engineering.

From 2006 to 2012, he was with Grundfos Research and Development China, Suzhou, China, as a Senior Motor Engineer, working on the design and analysis of the permanent magnet machine and devices. From 2016 to 2017, he was a Postdoctoral Researcher with the Department of Energy Technology, Aalborg University, where he has been an Assistant Professor, since 2017. His research interests include the design and control of synchronous reluctance and permanent magnet machines.

FREDE BLAABJERG (Fellow, IEEE) received the Ph.D. degree in electrical engineering from Aalborg University, in 1995. He is currently pursuing the Honorary degree (honoris causa) with Universitatea Politehnica Timisoara (UPT), Romania, and the Tallinn University of Technology, Estonia.

He was with ABB Scandia, Randers, Denmark, from 1987 to 1988. He became an Assistant Professor, in 1992, an Associate Professor, in 1996, and a Full Professor of power electronics and drives, in 1998. Since 2017, he has been a Villum Investigator. His current research interests include power electronics and its applications, such as in wind turbines, PV systems, reliability, harmonics, and adjustable speed drives. He has published more than 600 journal articles in the fields of power electronics and its applications. He is a coauthor of four monographs and an editor of ten books in power electronics and its applications.

Dr. Blaabjerg received the 32 IEEE Prize Paper Awards; the IEEE PELS Distinguished Service Award, in 2009; the EPE-PEMC Council Award, in 2010; the IEEE William E. Newell Power Electronics Award, in 2014; the Villum Kann Rasmussen Research Award, in 2014; the Global Energy Prize, in 2019; and the 2020 IEEE Edison Medal. He was the Editor-in-Chief of the IEEE TRANSACTIONS ON POWER ELECTRONICS, from 2006 to 2012. He has been the Distinguished Lecturer of the IEEE Power Electronics Society, from 2005 to 2007, and the IEEE Industry Applications Society, from 2010 to 2011 and from 2017 to 2018. From 2019 to 2020, he serves as the President of the IEEE Power Electronics Society. He is also the Vice President of the Danish Academy of Technical Sciences. He was nominated by Thomson Reuters to be between the most 250 cited researchers in Engineering in the world, from 2014 to 2018.